



Special Feature: Innovative Technologies for the Automotive Structure and Processing

Research Report

Efficient Direct Simulation Model of Fiber Motion in Molding Process of Discontinuous Fiber-reinforced Plastics

Toshiki Sasayama, Masahide Inagaki and Norikazu Sato

Report received on Oct. 7, 2019

■ABSTRACT■ For predicting the mechanical performance of products made of discontinuous fiber-reinforced thermoplastics, it is necessary to simulate the dynamic behavior of fibers during the molding process and predict the resulting fiber orientations, lengths, and dispersions within the product. For this purpose, this study develops an efficient simulation model for fiber motion in viscous shear flow based on the conventional model, in which a fiber is represented as a chain of connected spheres. The computational cost of the conventional model is significantly reduced by simplifying the equation of motion and reducing the number of spheres in the fiber model. In addition, a theoretically derived correction procedure is adopted to reproduce the results of the conventional model. The improved model is verified to be effective by a comparison with the conventional model and then applied to simulate fiber orientation in injection molding. Furthermore, the fiber length reduction in simple shear flow is simulated by implementing fiber breakage in the improved model. The simulations show that the improved model can be used to efficiently explore microscopic fiber behavior during the molding process. Since this behavior has not been clarified well, its simulation will be useful for improving the molding process to obtain better products.

■KEYWORDS■ Discontinuous Fiber-reinforced Plastics, Injection Molding, Numerical Modeling, Fiber Suspension, Microstructure

1. Introduction

Fiber-reinforced plastics are widely applied in automotive components as a lightweight material. For the mass production of components with complex geometry, discontinuous fiber-reinforced thermoplastics (FRTPs) are suitable because of their higher formability. Products made of discontinuous FRTPs are generally manufactured by injection or compression molding, in which the fibers experience forces due to interactions with the polymer flow, other fibers, and mold walls. These interactions result in an orientation distribution, deformation, and breakage of the fibers in the molded product. Because these factors strongly affect the warpage and mechanical performance of the product, it is desirable to control fiber behavior in the molding process by optimizing the molding conditions and mold design. However, because of the difficulty of experimentally observing fibers during and after molding, the molding process is improved by trial and error without understanding how the fibers are affected by the molding parameters

and correlated to product quality.

Numerical simulations can provide useful information for process improvement. Typically, a mold-filling simulation is first performed to predict the distributions of fiber orientation and length within the product, followed by a mechanical simulation to calculate mechanical performance based on the predicted fiber distributions. In general, the fiber orientation distribution is predicted by solving an evolution equation of the second-order orientation tensor⁽¹⁾ at each position in the mold. Fiber orientation models are typically constructed based on Jeffery's equation,⁽²⁾ which gives an analytical solution of the motion of a rigid ellipsoidal particle in viscous shear flow. For short fiber composites, the Folgar-Tucker model,⁽³⁾ which includes an isotropic rotary diffusion term to phenomenologically express the effect of fiber-fiber interactions, is widely used. For enhancing prediction accuracy and addressing long fiber composites, various improvements have been made, such as the incorporation of slow orientation⁽⁴⁾ and anisotropic rotary diffusion.^(5,6) The fiber length distribution

is predicted by calculating the time evolution of populations for each discretized fiber length while conserving the total fiber length.^(7,8) In these models, fiber breakage is judged to have occurred when the hydrodynamic force applied to the fiber exceeds the threshold and the buckling criterion is satisfied. These prediction models for fiber orientations and lengths have been implemented in commercial molding simulation software and applied to practical use. Although these models provide macroscopic quantities such as the fiber orientation tensor and the average fiber length throughout the whole molded product, they require some empirical model parameters, whose optimal values are generally difficult to obtain. In addition, the microscopic behavior of fiber orientation and breakage cannot be obtained using these models.

A particle-level simulation, which solves for the motion of individual fibers, can be used to identify the simulation parameters and improve the accuracy of the above-mentioned macroscopic prediction models. Furthermore, particle-level simulation enables us to understand the mechanism of fiber behavior in detail. Various particle-level simulation models have been proposed.⁽⁹⁻¹⁴⁾ A fiber is modeled as a chain of connected components, such as spheres, rods, and spheroids, and fiber motion is computed by solving the equation of motion for each component. For example, Yamamoto and Matsuoka⁽⁹⁾ developed a bead-chain model and applied it to simulate the suspension rheology⁽¹⁵⁾ and fiber breakage phenomenon in simple shear flow.⁽¹⁶⁾ Recently, as an application to a more practical molding process, a simulation of fiber dispersion behavior in a ribbed plate during compression molding using a mechanistic fiber model has been reported.⁽¹⁷⁾

However, simulating concentrated fiber suspensions using particle-level simulation models is still challenging because the models require a high computation time. Hence, the present study aims to establish an efficient particle-level simulation model. To this end, we improve the conventional bead-chain model by applying the following two steps. First, the equation of motion for each sphere is simplified (referred to as the simplified model). Second, the simplified model is further improved by reducing the number of spheres needed to model the fiber (the reduced model). Each step includes modifications for reproducing the results obtained using the conventional bead-chain model. To examine the validity of these improved models, fiber motion in simple shear flow is simulated.

Furthermore, the reduced model is applied to simulate fiber orientation in injection molding to investigate its applicability to complex flow fields. Finally, an application of the reduced model to fiber breakage simulation is briefly described.

2. Simulation Method

2.1 Conventional Model

In the conventional model,⁽⁹⁾ a fiber is modeled as a chain of interconnected spheres, as shown in Fig. 1(a). The following equations are solved for each sphere.

$$m \frac{d\mathbf{v}_i}{dt} = \mathbf{F}_i^h + \sum_{j=1} \mathbf{F}_{ij}^s + \sum_{j=1} \mathbf{f}_{ij} + \sum_{n=1} \mathbf{F}_{in}^p, \quad (1)$$

$$\frac{2}{5} ma^2 \frac{d\boldsymbol{\omega}_i}{dt} = \mathbf{T}_i^h + \sum_{j=1} \mathbf{T}_{ij}^b + \sum_{j=1} \mathbf{T}_{ij}^t + \sum_{j=1} (\mathbf{a}_{ij} \times \mathbf{f}_{ij}), \quad (2)$$

where i is the sphere number, j denotes the sphere connected to sphere i , n denotes the sphere not connected to sphere i , m is the mass of the sphere, a is the sphere radius, \mathbf{v}_i is the velocity of sphere i , $\boldsymbol{\omega}_i$ is the angular velocity of sphere i , \mathbf{F}_i^h is the hydrodynamic force, \mathbf{F}_{ij}^s is the stretching force, \mathbf{f}_{ij} is the shear force, \mathbf{F}_{in}^p is the particle-particle (fiber-fiber) interaction force, \mathbf{T}_i^h is the hydrodynamic torque, \mathbf{T}_{ij}^b is the bending torque, \mathbf{T}_{ij}^t is the twisting torque, and \mathbf{n}_{ij} is the unit vector from sphere i to sphere j . In addition,

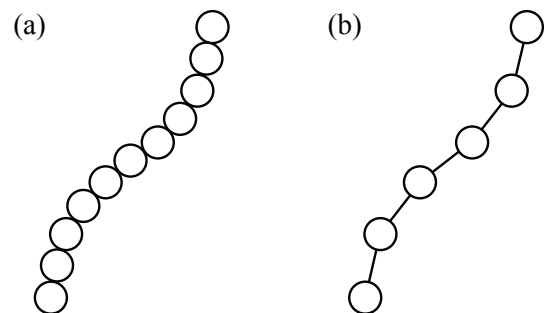


Fig. 1 Fiber modeling using interconnected spheres. (a) Conventional and simplified models, in which the number of spheres is equal to the fiber aspect ratio. (b) Reduced model, in which the fiber is discretized with fewer spheres.

the following equation needs to be solved to satisfy the no-slip condition between connected spheres.

$$\mathbf{v}_i + a\boldsymbol{\omega}_i \times \mathbf{n}_{ij} = \mathbf{v}_j + a\boldsymbol{\omega}_j \times \mathbf{n}_{ji}. \quad (3)$$

To solve these equations, the forces and the torques that exclude the terms of the shear force are first calculated. The shear force is then computed by solving the simultaneous linear equation obtained by substituting Eqs. (1) and (2) into an equation derived by taking the time derivative of Eq. (3). Finally, the position and orientation angle of the sphere are obtained using the velocity and angular velocity calculated using Eqs. (1) and (2).

Although the conventional model can represent fiber motion in detail, one needs to solve the simultaneous linear equation for the shear force and calculate both the position and orientation angle of each sphere. This makes the calculation of even short fibers computationally intensive. Moreover, when modeling a fiber with aspect ratio r_f , the number of spheres required to model the fiber is r_f (when r_f is an integer). Therefore, the simulation of long fiber suspensions significantly increases the computation time.

2.2 Model Improvements

We propose an efficient model that is based on the conventional model and can reproduce its results. The procedure for the model improvement is briefly described below. The details can be found in our previous reports.⁽¹⁸⁻²⁰⁾

2.2.1 Simplified Model

In the simplified model,⁽¹⁸⁾ the effects of the bending and hydrodynamic torques, which are considered in Eq. (2), are included in Eq. (1) as additional terms. Torsional motion is neglected in this model, which is a reasonable assumption (see Sec. 3.2). With this simplification, we only need to solve the equation of translational motion and calculate the resulting sphere positions; the calculation of the sphere orientation angles is not necessary, which enhances both computational efficiency and numerical stability. The resulting equation of translational motion is given as

$$m \frac{d\mathbf{v}_i}{dt} = \mathbf{F}_i^h + \sum_{j=1} \mathbf{F}_{ij}^s + \sum_{n=1} \mathbf{F}_{in}^p + \sum_{j=1} \mathbf{F}_{ij}^b + \sum_{j=1} \mathbf{F}_{ij}^{ht}, \quad (4)$$

where \mathbf{F}_{ij}^b and \mathbf{F}_{ij}^{ht} are the forces converted from the bending and hydrodynamic torques, respectively. In this model, the bending torque at each position within the fiber is calculated using the flexural rigidity and radius of curvature of the fiber. The angular velocity of the spheres is required for calculating the hydrodynamic torque, but it cannot be directly obtained because the simplified model does not solve the equation of rotational motion, unlike the conventional model (Eq. (2)). Therefore, the angular velocity is approximated using the following equation.

$$\frac{\boldsymbol{\omega}_i + \boldsymbol{\omega}_j}{2} = \frac{\mathbf{r}_{ij} \times (\mathbf{v}_j - \mathbf{v}_i)}{|\mathbf{r}_{ij}|^2}, \quad (5)$$

where \mathbf{r}_{ij} is the vector from sphere i to sphere j . This equation is derived by combining Eq. (3) and the assumption that the twisting motion of the sphere can be ignored. By calculating the right-hand side of Eq. (5), we obtain the average angular velocity of spheres i and j .

2.2.2 Reduced Model

The simplified model, which uses r_f spheres for modeling a fiber with aspect ratio r_f , is further modified⁽¹⁹⁾ to discretize the fiber with fewer spheres, as shown in Fig. 1(b). For convenience, the term “segment” is used to describe the discretization of the fiber. A segment consists of two spheres and one massless rod connecting the spheres. For example, the number of segments N^{seg} of the fiber in Fig. 1(b) is 5.

A fiber with fewer spheres, referred to as a reduced fiber, does not show the same motion as a fiber modeled with r_f spheres because of the differences in mass, moment of inertia, and total force and torque applied to the fiber.⁽¹⁹⁾ Hence, we introduce correction factors for the forces exerted on the spheres to reduce the numerical errors caused by these differences. For deriving the correction factors, we first consider a fiber modeled with r_f spheres that has the same shape as that of the reduced fiber. This fiber is referred to as an unreduced fiber. We then construct the equations of translational and rotational motions for the reduced and unreduced fibers. In this step, because the unreduced fiber has spheres not included in the reduced fiber, the forces on these spheres need to be calculated. This calculation is performed only for the hydrodynamic force because the hydrodynamic force

is distributed along the segment and has a non-zero value, whereas the other forces in Eq. (4) cancel out or are regarded to be zero. The hydrodynamic forces on the spheres in the unreduced fiber are calculated by linearly interpolating the forces on the spheres in the reduced fiber. Finally, the correction factors are determined so that the equations for these two fibers become equivalent. Because of the difference in the above-mentioned calculation process of forces when constructing the equations of motion, the correction factor for a force depends on whether the force is distributed along the segment.

The equation of motion for sphere i in the reduced model is given by

$$m \frac{d\mathbf{v}_i}{dt} = \alpha^T (\mathbf{F}_i^{\text{ND}} \cdot \mathbf{n}_i^{\text{G}}) \mathbf{n}_i^{\text{G}} + \alpha^R \{ \mathbf{F}_i^{\text{ND}} - (\mathbf{F}_i^{\text{ND}} \cdot \mathbf{n}_i^{\text{G}}) \mathbf{n}_i^{\text{G}} \} + \beta_i^T (\mathbf{F}_i^{\text{D}} \cdot \mathbf{n}_i^{\text{G}}) \mathbf{n}_i^{\text{G}} + \beta_i^R \{ \mathbf{F}_i^{\text{D}} - (\mathbf{F}_i^{\text{D}} \cdot \mathbf{n}_i^{\text{G}}) \mathbf{n}_i^{\text{G}} \}, \quad (6)$$

where \mathbf{n}_i^{G} is the unit vector from the mass center of the fiber to sphere i , α^T , α^R , β_i^T , and β_i^R are the correction factors, and \mathbf{F}_i^{ND} and \mathbf{F}_i^{D} are the forces, obtained as

$$\mathbf{F}_i^{\text{ND}} = \sum_{j=1} \mathbf{F}_{ij}^{\text{s}} + \sum_{ns=1} \mathbf{F}_{i ns}^{\text{p}} + \sum_{j=1} \mathbf{F}_{ij}^{\text{b}} + \sum_{j=1} \mathbf{F}_{ij}^{\text{ht}}, \quad (7)$$

$$\mathbf{F}_i^{\text{D}} = \mathbf{F}_i^{\text{h}}. \quad (8)$$

The superscripts ND and D denote “non-distributed” and “distributed”, respectively (see derivation process above). The calculation procedure for the particle-particle (fiber-fiber) interaction force $\mathbf{F}_{i ns}^{\text{p}}$ is as follows. The interaction force in the reduced model is calculated by considering the interaction between segments, in contrast to the sphere-sphere interactions in the simplified model. Hence, the interaction force between segments is and ns is first calculated. With segment is composed of spheres i and j , the interaction force applied to segment is from segment ns is distributed to both spheres i and j .

3. Results and Discussion

3.1 Motion of Single Fiber in Simple Shear Flow

The period of rotation of a rigid fiber with radius $a = 5 \mu\text{m}$ subjected to simple shear flow was first investigated. The shear rate and viscosity were set

to $\dot{\gamma} = 100 \text{ s}^{-1}$ and $\eta = 100 \text{ Pa}\cdot\text{s}$, respectively. The fiber was initially oriented in the flow direction and thus exhibited in-plane rotation. **Figure 2** shows the period of rotation as a function of the fiber aspect ratio calculated using the conventional model and the two proposed models. $N^{\text{seg}} = 1$ was used for the calculation with the reduced model. The vertical axis represents the dimensionless period of rotation, defined as the product of the period of rotation T and the shear rate $\dot{\gamma}$. The conventional model predicts a linear increase in the period of rotation as the aspect ratio increases, which is well traced by the proposed models. Here, although $N^{\text{seg}} = 1$ is employed for the reduced model in Fig. 2, an arbitrary number of segments, in the range of $1 \leq N^{\text{seg}} \leq r_f - 1$, can be used in the model. We investigated the effect of the number of segments on the rotation period of a fiber with $r_f = 100$ and found that the relative errors between the simplified and reduced models were smaller than 0.001% for various N^{seg} .

In these calculations, the computational efficiency of the simplified model compared to that of the conventional model increases in proportion to the aspect ratio r_f ; the simplified model was ten times faster for $r_f = 100$. A comparison between the simplified and reduced models is shown in **Fig. 3**, which plots the speed-up ratio of the reduced model compared to the simplified model for $r_f = 100$ as a function of the number of segments. Reducing the number of segments in the fiber greatly enhances the computational efficiency

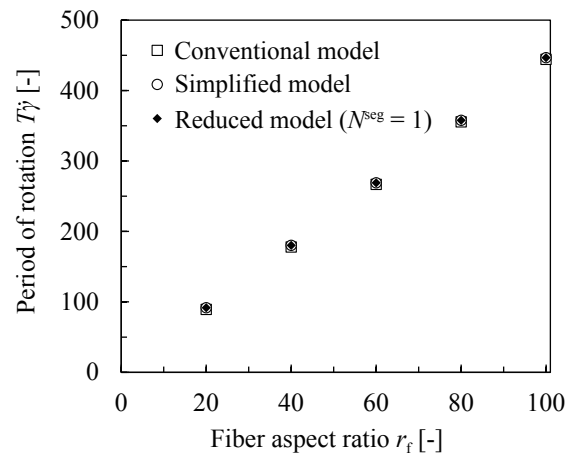


Fig. 2 Period of rotation of the fiber as a function of the fiber aspect ratio simulated by conventional, simplified, and reduced models.

of the reduced model. Provided that the fiber is rigid, the number of segments can be reduced to $N^{\text{seg}} = 1$ for maximum efficiency. These results reveal that the proposed models can reproduce the motion of a rigid fiber calculated using the conventional model with much lower computation time.

Next, the motion of a single flexible fiber in simple shear flow was examined. The flexibility of the fiber was varied by changing the Young's modulus of the fiber E_f . **Figure 4** shows snapshots of the flexible fiber with $E_f = 0.1$ GPa, and plots the trajectories of the sphere located at the end of the fiber with $E_f = 0.1$ and 0.02 GPa calculated using the conventional and simplified models. The snapshots show the fiber deformation observed at the time marked with red circles on the trajectory. In simple shear flow, a flexible fiber, which has an intrinsically straight shape, exhibits S-shaped deformation, as shown in Fig. 4. A decrease in Young's modulus leads to larger fiber deformation, resulting in a different trajectory. The simplified model well reproduces the trajectories simulated using the conventional model, which verifies that the proposed model is applicable to flexible fibers as well as rigid fibers. We also compared the motion of the flexible fiber ($r_f = 50$ and $E_f = 0.5$ GPa) simulated using the simplified and reduced models (**Fig. 5**). The reduced model ($N^{\text{seg}} = 25$ and 15) well captures the fiber deformation and rotation predicted by the simplified model ($N^{\text{seg}} = 49$).

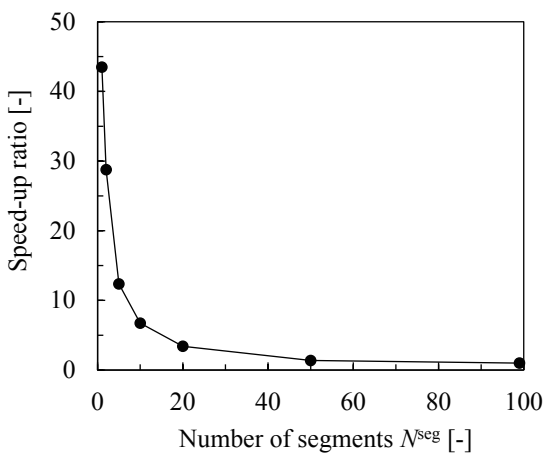


Fig. 3 Ratio of calculation time for simplified model to that for reduced model as a function of number of segments.

3. 2 Orientation Behavior of Fiber Suspensions in Simple Shear Flow

Fiber suspensions in simple shear flow were simulated considering fiber-fiber interactions. The calculation was performed in a cubic computational domain, where the top and bottom planes in the z direction were moving walls and periodic boundary conditions were employed in the x and y directions. The fiber radius, shear rate, and viscosity of fluid were same as those in the previous section.

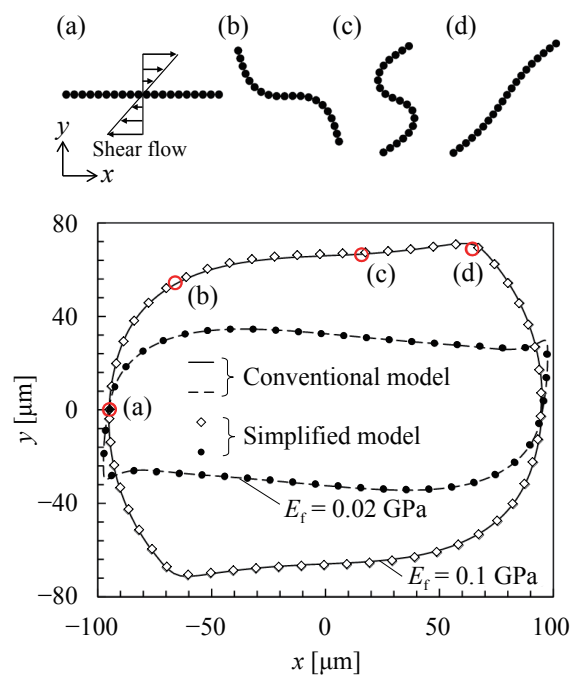


Fig. 4 Snapshot of flexible fiber motion with $r_f = 20$ and $E_f = 0.1$ GPa (top). Trajectories of the sphere at the fiber end for two Young's modulus values (bottom).

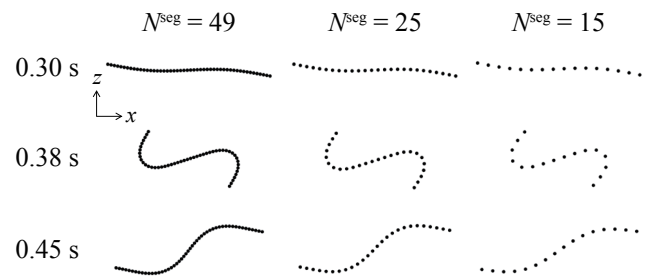


Fig. 5 Snapshots of flexible fiber motion ($r_f = 50$ and $E_f = 0.5$ GPa) simulated with three different numbers of segments.

A flexible-fiber suspension was investigated using the conventional and simplified models. **Figure 6(a)** shows the time evolutions of the fiber orientation tensor components A_{xx} and A_{yy} . Figure 6(b) shows the microstructure of the fibers obtained at a strain of 45. The aspect ratio r_f , Young's modulus E_f , and volume fraction V_f of the fiber were set to 20, 0.1 GPa, and 0.075, respectively. The fibers were initially randomly oriented and thus the orientation tensor components A_{xx} and A_{yy} were approximately 1/3 (A_{zz} had the same value). As the applied strain increases, the fibers become oriented in nearly the flow direction and the component A_{xx} varies roughly in the range of 0.8-0.9. At the early stage in Fig. 6(a), the orientation tensor components exhibit periodic oscillation because most of fibers at this stage tend to rotate simultaneously because the fiber-fiber interactions do not sufficiently disturb the fiber rotation periods. The oscillation is gradually

damped as the applied strain increases and the effect of the interactions on fiber motion becomes larger. A comparison of the orientation tensor components in Fig. 6(a) between the two models indicates that the simplified model produces a fiber orientation that well matches that obtained using the conventional model despite the occurrence of the complicated deformation shown in Fig. 6(b).

Figure 7 compares the simplified and reduced models in terms of the variation of the orientation

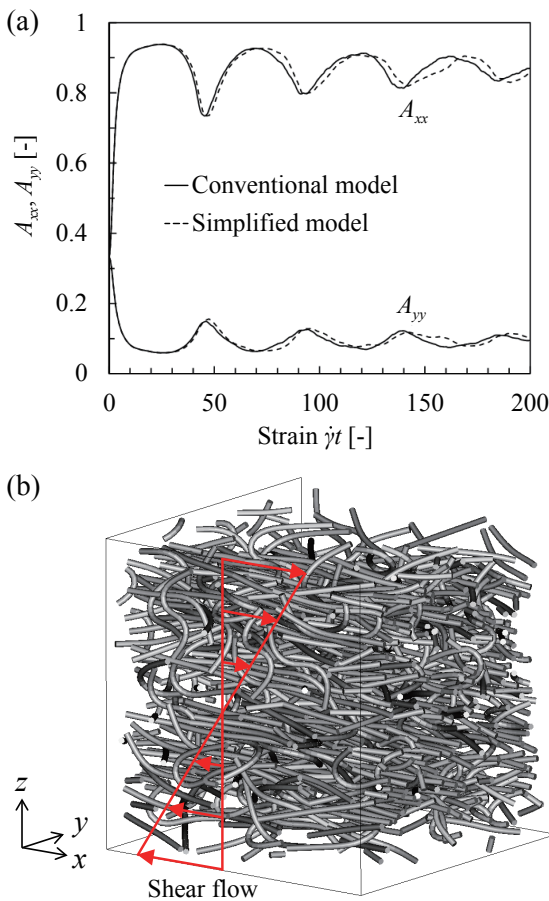


Fig. 6 (a) Time evolution of fiber orientation tensor components A_{xx} and A_{yy} simulated using conventional and simplified models. (b) Microstructure of the flexible fiber suspension at strain of 45.

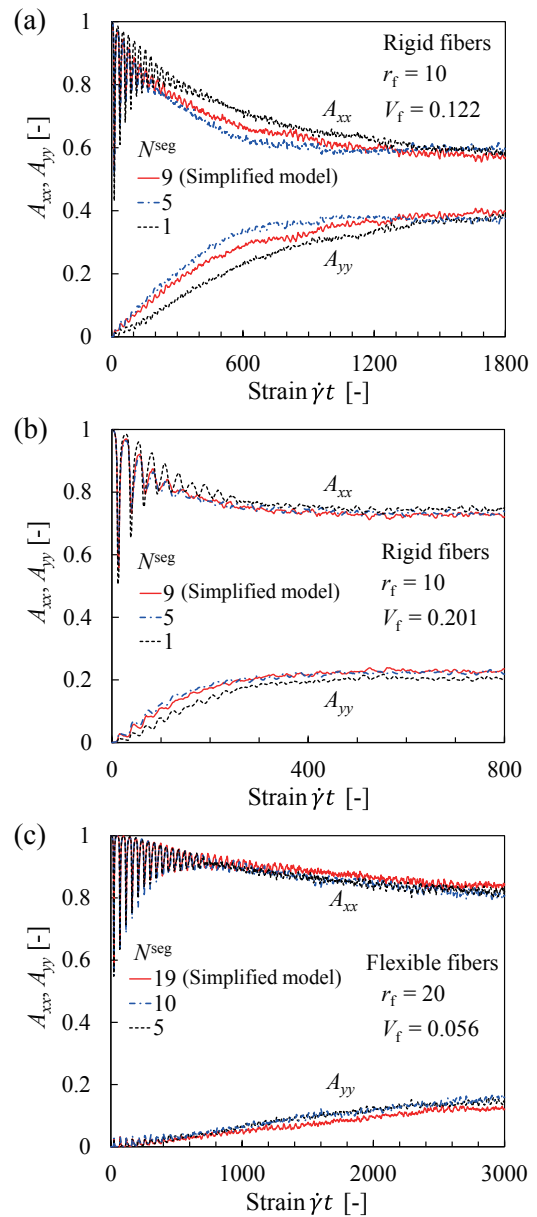


Fig. 7 Time evolution of fiber orientation tensor components A_{xx} and A_{yy} simulated using simplified and reduced models for various conditions.

tensor components as a function of applied shear strain for three conditions, with the aspect ratio, volume fraction, and flexibility of fibers varied. In these simulations, fibers were initially oriented in the flow direction, unlike the case in Fig. 6. The reduced model ($N^{\text{seg}} < r_f - 1$) well reproduces the time evolution of the orientation simulated using the simplified model ($N^{\text{seg}} = r_f - 1$) for the three conditions.

3.3 Fiber Orientations in Injection Molding Process

The orientation behavior of fibers in the injection molding process was simulated using the proposed models and considering fiber-fiber interactions. We first performed a mold-filling simulation of the plaque-shaped mold shown in Fig. 8 using the commercial molding simulation software 3D TIMON (Toray Engineering, Tokyo, Japan) to obtain the time series of the velocity and viscosity fields of polypropylene containing 40 wt% long glass fibers. The injection speed was set to 10 cm³/s. The inlet and mold temperatures were held at 230°C and 110°C, respectively. Only the mold-filling stage was simulated; the packing and cooling stages were not calculated. The flow data were then used to calculate the motion of fibers whose radius a , aspect ratio r_f , and Young's modulus E_f were 10 μm, 50, and 70 GPa, respectively. Until the end of the mold filling, fibers oriented in the flow direction were generated continuously at the inlet to make the fiber volume fraction $V_f = 0.1$. After the simulation of fiber motion during the molding process, the fiber orientation tensor A_{ij} was calculated at a position 95 mm downstream from the inlet (the region marked with dotted lines in Fig. 8).

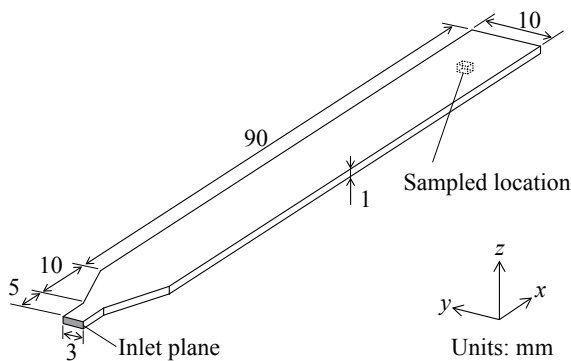


Fig. 8 Dimensions of injection-molded plaque model. The fiber orientation tensor is calculated within the region marked with dotted lines.

Figure 9 shows the distributions of the fiber orientation components in the thickness direction obtained using the simplified and reduced models at the sampled location. The plots at the point near the walls ($z = \pm 0.5$ mm) are omitted because there were insufficient segments for calculating the orientation tensor. The orientation tensor distribution shows a multilayer (shell-core) structure, in which the fibers in the middle (core) layer are less aligned in the flow direction and exhibit a random in-plane orientation, whereas those in the shell layers surrounding the core layer are mainly parallel to the flow direction. Figure 10 shows the fibers in the sampled region of 1.2 mm × 1.2 mm × 1.0 mm simulated using the reduced

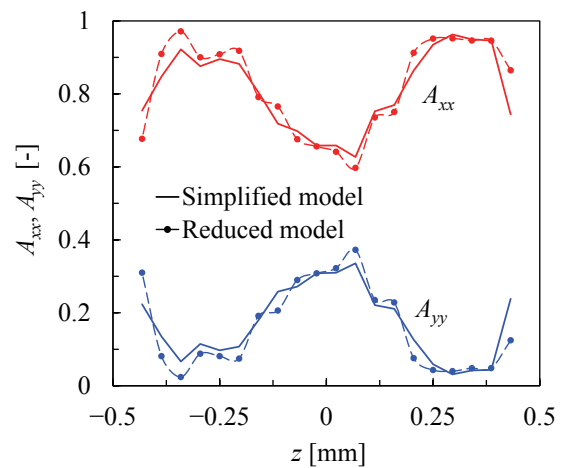


Fig. 9 Distribution of fiber orientation tensor components A_{xx} and A_{yy} in the thickness direction.

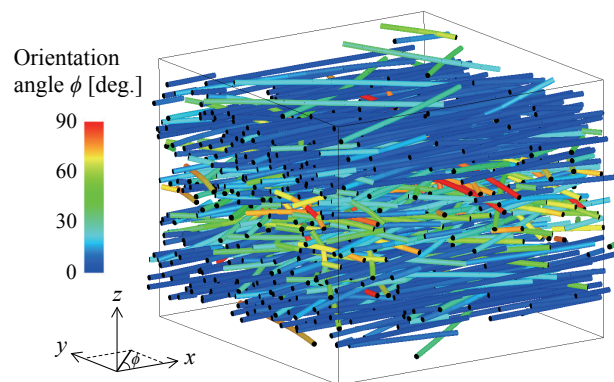


Fig. 10 Fiber orientations at the sampled location. Segments are color-coded according the orientation angle ϕ between the x -axis and the direction vector of the segment projected on the x - y plane.

model. The segments are color-coded according to the angle between the x -axis and the projection of their direction vectors on the x - y plane. The layered structure of the fiber orientation can be clearly observed. The profile of the structure varies with the processing conditions and mold geometry.⁽²¹⁾ A comparison of the results of the simplified and reduced models in Fig. 9 indicates that the orientation tensors predicted by the two models are in good agreement, revealing that the reduced model works well even in a complicated flow field, such as that in the injection molding process.

3.4 Application to Prediction of Fiber Length Degradation

The proposed models can be applied to simulate fiber length degradation by implementing a fiber breakage model.⁽²⁰⁾ To express fiber breakage, the connection between the spheres is removed at the position where the bending stress exceeds the tensile strength of the fiber. Moreover, statistically distributed tensile strengths are assigned to the segments of the fibers to consider the variation in fiber strength. **Figure 11** shows snapshots of the breakage behavior of glass fibers in simple shear flow with $\dot{\gamma} = 100 \text{ s}^{-1}$ and $\eta = 100 \text{ Pa}\cdot\text{s}$ simulated using the reduced model. The fiber volume fraction and initial fiber length were 0.1 and 2 mm, respectively. As in Sec. 3.2, the periodic boundary condition and wall boundaries were employed. The fibers are color-coded according to their length. In Figs. 11(a)-(c), the fibers with an initial length of 2 mm exhibit large deformation and breakage due to the forces exerted by the fluid and fiber-fiber interactions. Using the results in Fig. 11, we calculated the average fiber length and fiber length distribution.

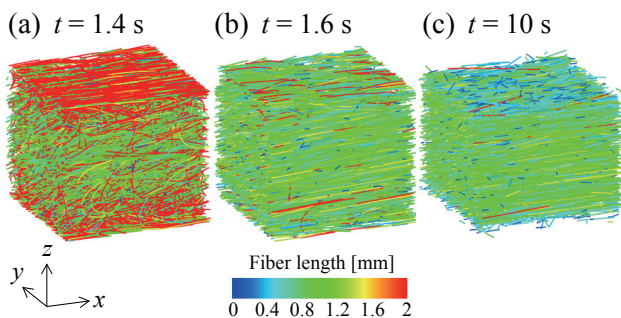


Fig. 11 Breakage behavior of fibers at various time instances. Fibers are color-coded according to their length.

Figure 12(a) shows the weight-averaged fiber length as a function of time. Because the initial fiber orientation was set to be aligned in the flow direction in this calculation, most of the fibers simultaneously start to rotate, deform, and break, which results in a drastic drop in the average fiber lengths from $t = 1.3 \text{ s}$ to 1.6 s . The decrease rate of fiber length is much smaller after $t = 1.6 \text{ s}$ because as the fiber length decreases, the fiber stiffness becomes relatively large and the fibers tend to exhibit less breakage. The average fiber length is almost at a steady state at $t = 10 \text{ s}$. **Figure 12(b)** shows the fiber length distribution at this time. The distribution has a maximum at about 0.8 mm. Note that the decrease rate and convergence value of the fiber length are affected by various factors, such as fiber stiffness, strength, orientation, volume fraction, and fluid shear stress. For example, the effect of the fiber volume fraction is shown in **Fig. 13**. It can be seen that an increase in the fiber volume fraction results in

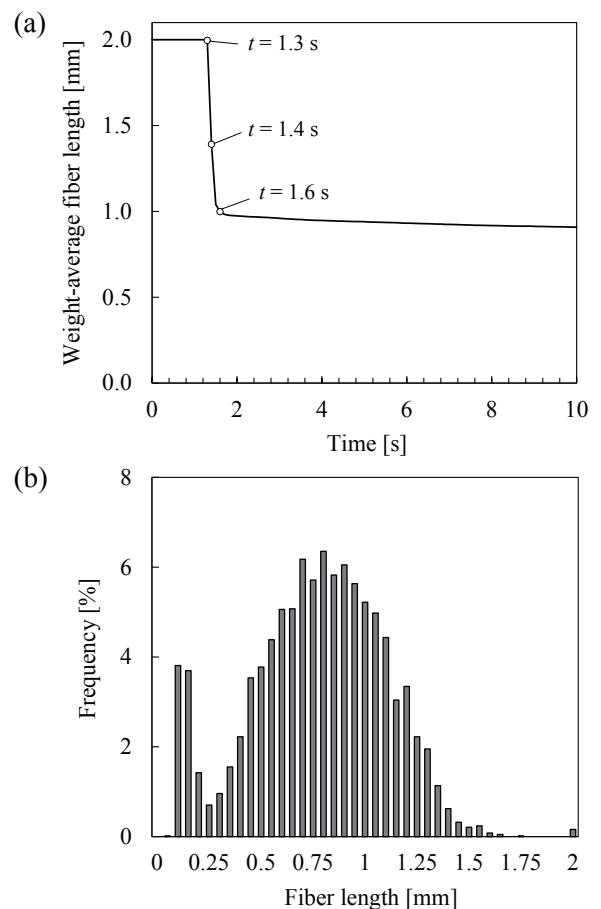


Fig. 12 (a) Time evolution of weight-average fiber length. (b) Fiber length distribution at $t = 10 \text{ s}$.

lower fiber length. This is because even shorter fibers can break due to the increased fiber-fiber interactions.

4. Conclusions

This study improved the particle-level simulation method developed by Yamamoto and Matsuoka,⁽⁹⁾ in which interconnected spheres are used for modeling a fiber. The computational cost of this conventional model was reduced using the following two modifications. First, the bending and hydrodynamic torques, which are considered in the equation of rotational motion, were included in the equation of translational motion as additional terms. This simplified model does not need to solve the equation of rotational motion. Second, the number of spheres used to discretize the fiber was reduced. In this reduced model, the forces for the spheres were multiplied by theoretically derived correction factors to reproduce the results of the simplified model. An investigation of fiber motion in simple shear flow revealed that the simplified model well reproduced the results of the conventional model. In addition, the reduced model was verified to reproduce fiber motion in both simple shear flow and the complicated flow in injection molding simulated using the simplified model. Finally, the reduced model was applied to simulate the breakage of fibers subjected to simple shear flow. The fiber deformation and breakage were induced by the forces exerted by the fluid and the fiber-fiber interactions, resulting in a fiber length

reduction. These investigations verified the effectiveness of the proposed particle-level simulation model, which will be a useful tool for efficiently simulating and understanding fiber behavior in the manufacturing process of discontinuous fiber-reinforced plastics.

References

- (1) Advani, S. G. and Tucker III, C. L., "The Use of Tensors to Describe and Predict Fiber Orientation in Short Fiber Composites", *J. Rheol.*, Vol. 31, No. 8 (1987), pp. 751-784.
- (2) Jeffery, G. B., "The Motion of Ellipsoidal Particles Immersed in a Viscous Fluid", *Proc. R. Soc. A*, Vol. 102, No. 715 (1922), pp. 161-179.
- (3) Folgar, F. and Tucker III, C. L., "Orientation Behavior of Fibers in Concentrated Suspensions", *J. Reinf. Plast. Compos.*, Vol. 3, No. 2 (1984), pp. 98-119.
- (4) Wang, J., O'Gara, J. F. and Tucker III, C. L., "An Objective Model for Slow Orientation Kinetics in Concentrated Fiber Suspensions: Theory and Rheological Evidence", *J. Rheol.*, Vol. 52, No. 5 (2008), pp. 1179-1200.
- (5) Phelps, J. H. and Tucker III, C. L., "An Anisotropic Rotary Diffusion Model for Fiber Orientation in Short- and Long-fiber Thermoplastics", *J. Non-Newtonian Fluid Mech.*, Vol. 156, No. 3 (2009), pp. 165-176.
- (6) Tseng, H.-C., Chang, R.-Y. and Hsu, C.-H., "An Objective Tensor to Predict Anisotropic Fiber Orientation in Concentrated Suspensions", *J. Rheol.*, Vol. 60, No. 2 (2016), pp. 215-224.
- (7) Durin, A., De Micheli, P., Ville, J., Inceoglu, F., Valette, R. and Vergnes, B., "A Matricial Approach of Fibre Breakage in Twin-screw Extrusion of Glass Fibres Reinforced Thermoplastics", *Composites, Part A*, Vol. 48 (2013), pp. 47-56.
- (8) Phelps, J. H., El-Rahman, A. I. A., Kunc, V. and Tucker III, C. L., "A Model for Fiber Length Attrition in Injection-molded Long-fiber Composites", *Composites, Part A*, Vol. 51 (2013), pp. 11-21.
- (9) Yamamoto, S. and Matsuoka, T., "A Method for Dynamic Simulation of Rigid and Flexible Fibers in a Flow Field", *J. Chem. Phys.*, Vol. 98, No. 1 (1993), pp. 644-650.
- (10) Ross, R. F. and Klingenberg, D. J., "Dynamic Simulation of Flexible Fibers Composed of Linked Rigid Bodies", *J. Chem. Phys.*, Vol. 106, No. 7 (1997), pp. 2949-2960.
- (11) Fan, X., Phan-Thien, N. and Zheng, R., "A Direct Simulation of Fibre Suspensions", *J. Non-Newtonian Fluid Mech.*, Vol. 74, No. 1-3 (1998), pp. 113-135.
- (12) Schmid, C. F., Switzer, L. H. and Klingenberg, D. J., "Simulations of Fiber Flocculation: Effects of Fiber Properties and Interfiber Friction", *J. Rheol.*, Vol. 44, No. 4 (2000), pp. 781-809.

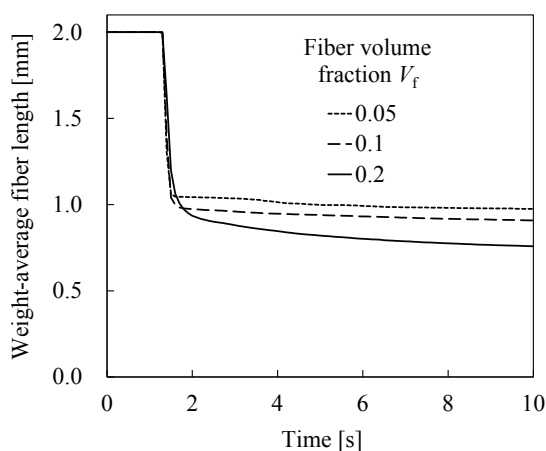


Fig. 13 Time evolution of weight-averaged fiber length for various fiber volume fractions.

- (13) Joung, C. G., Phan-Thien, N. and Fan, X. J., "Direct Simulation of Flexible Fibers", *J. Non-Newtonian Fluid Mech.*, Vol. 99, No. 1 (2001), pp. 1-36.
- (14) Londoño-Hurtado, A., Osswald, T. A. and Hernandez-Ortiz, J. P., "Modeling the Behavior of Fiber Suspensions in the Molding of Polymer Composites", *J. Reinf. Plast. Compos.*, Vol. 30, No. 9 (2011), pp. 781-790.
- (15) Yamamoto, S. and Matsuoka, T., "Dynamic Simulation of Fiber Suspensions in Shear Flow", *J. Chem. Phys.*, Vol. 102, No. 5 (1995), pp. 2254-2260.
- (16) Yamamoto, S. and Matsuoka, T., "Dynamic Simulation of Flow-induced Fiber Fracture", *Polym. Eng. Sci.*, Vol. 35, No. 12 (1995), pp. 1022-1030.
- (17) Kuhn, C., Walter, I., Täger, O. and Osswald, T. A., "Simulative Prediction of Fiber-matrix Separation in Rib Filling during Compression Molding Using a Direct Fiber Simulation", *J. Compos. Sci.*, Vol. 2, No. 1 (2018), Article No. 2.
- (18) Sasayama, T. and Inagaki, M., "Simplified Bead-chain Model for Direct Fiber Simulation in Viscous Flow", *J. Non-Newtonian Fluid Mech.*, Vol. 250 (2017), pp. 52-58.
- (19) Sasayama, T. and Inagaki, M., "Efficient Bead-chain Model for Predicting Fiber Motion during Molding of Fiber-reinforced Thermoplastics", *J. Non-Newtonian Fluid Mech.*, Vol. 264 (2019), pp. 135-143.
- (20) Sasayama, T., Inagaki, M. and Sato, N., "Direct Simulation of Glass Fiber Breakage in Simple Shear Flow Considering Fiber-fiber Interaction", *Composites, Part A*, Vol. 124 (2019), 105514.
- (21) Papathanasiou, T. D., "Flow-induced Alignment in Injection Molding of Fiber-reinforced Polymer Composites", *Flow-induced Alignment in Composite Materials*, Ed. by Papathanasiou, T. D. and Guell, D. C. (1997), pp. 112-165, Woodhead Publishing.

Figs. 3 and 7

Reprinted from *J. Non-Newtonian Fluid Mech.*, Vol. 264 (2019), pp. 135-143, Sasayama, T. and Inagaki, M., Efficient Bead-chain Model for Predicting Fiber Motion during Molding of Fiber-reinforced Thermoplastics, © 2018 Elsevier, with permission from Elsevier.

Fig. 6

Reprinted from *J. Non-Newtonian Fluid Mech.*, Vol. 250 (2017), pp. 52-58, Sasayama, T. and Inagaki, M., Simplified Bead-chain Model for Direct Fiber Simulation in Viscous Flow, © 2017 Elsevier, with permission from Elsevier.

Figs. 11, 12(a) and 13

Reprinted from *Composites, Part A*, Vol. 124 (2019), 105514, Sasayama, T., Inagaki, M. and Sato, N., "Direct Simulation of Glass Fiber Breakage in Simple Shear Flow Considering Fiber-fiber Interaction, © 2019 Elsevier, with permission from Elsevier.

Toshiki Sasayama

Research Field:

- Process Simulation for Fiber-reinforced Thermoplastics

Academic Societies:

- The Japan Society for Composite Materials
- The Japan Society of Polymer Processing



Masahide Inagaki

Research Fields:

- Numerical Analysis of Heat and Mass Transfer in Fuel Cell, Manufacturing Process and Cooling System
- Computational Fluid Dynamics
- Turbulence Modeling

Academic Degree: Dr.Eng.

Academic Societies:

- The Japan Society of Mechanical Engineers
- The Japan Society of Fluid Mechanics
- The Heat Transfer Society of Japan

Awards:

- JSME Medal for Outstanding Paper, The Japan Society of Mechanical Engineers, 2003, 2014
- Best Author Award from JSIAM, The Japan Society for Industrial and Applied Mathematics, 2006



Norikazu Sato

Research Fields:

- Process Simulation for Fiber-reinforced Thermoplastics
- Computational Fluid Dynamics

Academic Degree: Ph.D.

Academic Societies:

- The Japan Society of Mechanical Engineers
- The Japan Society of Fluid Mechanics

Award:

- JSME Medal for Outstanding Paper, The Japan Society of Mechanical Engineers, 2014

